Princeton Plasma Physics Laboratory

PPPL-3954rev

PPPL-3954rev

Observation of a High Performance Operating Regime with Small Edge-localized Modes in the National Spherical Torus Experiment

R. Maingi, K. Tritz, E.D. Fredrickson, J.E. Menard, S.A. Sabbagh, D. Stutman, M.G. Bell, R.E. Bell, C.E. Bush, D.A. Gates, D.W. Johnson, R. Kaita, S.M. Kaye, H.W. Kugel, B.P. LeBlanc, D. Mueller, R. Raman, A.L. Roquemore, and V.A. Soukhanovskii

Revised October 2004

PPPL
PRINCETON PLASMA PHYSICS LABORATORY

Prepared for the U.S. Department of Energy under Contract DE-AC02-76CH03073.

PPPL Report Disclaimers

Full Legal Disclaimer

Trademark Disclaimer

PPPL Report Availability

This report is posted on the U.S. Department of Energy's Princeton Plasma Physics Laboratory Publications and Reports web site in Fiscal Year 2005. The home page for PPPL Reports and Publications is: http://www.pppl.gov/pub_report/

Office of Scientific and Technical Information (OSTI):

Available electronically at: http://www.osti.gov/bridge.

Available for a processing fee to U.S. Department of Energy and its contractors, in paper from:

U.S. Department of Energy
Office of Scientific and Technical Information
P.O. Box 62
Oak Ridge, TN 37831-0062

Telephone: (865) 576-8401

Fax: (865) 576-5728

E-mail: reports@adonis.osti.gov

National Technical Information Service (NTIS):

This report is available for sale to the general public from:

U.S. Department of Commerce
National Technical Information Service
5285 Port Royal Road
Springfield, VA 22161

Telephone: (800) 553-6847

Fax: (703) 605-6900

Email: orders@ntis.fedworld.gov

Online ordering: http://www.ntis.gov/ordering.htm

Observation of a High Performance Operating Regime with Small Edge-Localized Modes in the National Spherical Torus Experiment

R. Maingi[a], K. Tritz[b], E.D. Fredrickson[c], J.E. Menard[c], S.A. Sabbagh[d], D. Stutman[b], M.G. Bell[c], R.E. Bell[c], C.E. Bush[a], D.A. Gates[c], D.W. Johnson[c], R. Kaita[c], S.M. Kaye[c], H.W. Kugel[c], B.P. LeBlanc[c], D. Mueller[c], R. Raman[e], A.L. Roquemore[c], V.A. Soukhanovskii[f]

[a]*Oak Ridge National Laboratory, Oak Ridge TN, 37831 USA*
[b]*Johns Hopkins University, Baltimore, MD, USA*
[c]*Princeton Plasma Physics Laboratory, PO Box 451, Princeton, NJ, 08543 USA*
[d]*Columbia University, New York, NY, USA*
[e]*University of Washington, Seattle WA, USA*
[f]*Lawrence Livermore National Laboratory, Livermore CA USA*

PACS numbers: 52.55.Fa, 52.55.Rk

Abstract

We report observation of a high performance scenario in the National Spherical Torus Experiment with very small edge-localized modes (ELMs). These ELMs individually have no measurable impact on stored energy but are observed by several diagnostics. The small ELMs have clear differences as compared with the ELM types reported in the literature, and this operating mode has distinct features compared with other high performance tokamak scenarios with little or no ELMs. The ELM is termed as 'Type V' and it has a short-lived n=1 magnetic pre-cursor oscillation rotating counter to the plasma current and. If extrapolable, this scenario would provide an attractive operating regime for next step fusion experiments.

I. Introduction

The search for high performance operating regimes with few or no edge localized modes (ELMs) has been a high priority in nuclear fusion research. The baseline operating scenario for the International Thermonuclear Experimental Reactor (ITER) relies on H-Mode confinement and profiles[1]. In most H-mode discharges in conventional aspect ratio tokamaks, ELMs are observed, which serve to flush fuel and impurity particles from the edge plasma into the scrape-off layer and divertor plasma. This periodic edge ejection results in transiently high power and particle loads to the plasma facing components (PFC). The best plasma performance is often realized in the Type I ELM regime (which is ITER's baseline scenario), but the type I ELM typically results in larger heat pulses than other ELM types[2]. Such transient PFC loading is tolerable in present day machines, but extrapolations show severe PFC damage resulting in larger, higher power density machines (such as ITER) when the ELM power loading exceeds material dependent limits[3].

Several high performance regimes either without ELMs or with little ELMs have been identified in conventional aspect ratio tokamaks. The Quiescent H-mode (QH-Mode) is a high performance, largely ELM-free regime discovered[4] on the DIII-D tokamak and recently reproduced in other devices. The QH-mode scenario requires neutral beam injection (NBI) counter to the direction of plasma current (I_p), low density, and relies on the presence of an edge harmonic oscillation for particle control. The Enhanced D_{α} (EDA) H-mode has been identified by the Alcator C-MOD group, and it relies on a quasi-coherent MHD mode in the vicinity of the separatrix for particle control[5]. The EDA H-mode bears strong resemblance to the earlier PDX forced density rise scenario, another high performance scenario with small/no ELMs[6], and the more recent high recycling steady (HRS) H-mode in JFT-2M[7]. Access to small ELMs was also reported at high triangularity[8] or poloidal beta (β_p)[9] in JT-60U. We note also the recent success at generating high performance discharges with no/few large ELMs using a stochastic boundary layer in DIII-D, which also provided good density control[10]. The operating regime achieved in the National Spherical Torus Experiment (NSTX) and reported here is distinct from all of these: 1) there is no counter injection or edge harmonic oscillation as in QH-mode, 2) there is no quasi-coherent mode in the edge

plasma as in EDA or related H-mode scenarios, 3) the β_p threshold needed to access this small ELM regime is ≥ 0.6 and no enhanced plasma shaping was required, and 4) no stochastic boundary technique was used to suppress ELMs. In addition the ELM characteristics and pre-cursors appear significantly different from existing ELM types in the literature and other ELM types observed in NSTX. Hence this regime provides another small ELM regime for possible use in large fusion devices to provide density control without the significant heat flux transients associated with conventional type I ELMs and without the performance degradation observed in Type III ELMs[11] (i.e. no degradation comparing type I and the small ELM discharges in NSTX). We refer to the perturbations in NSTX as type V ELMs (note that a low density branch[12] of the traditionally high density type III ELMs was observed in DIII-D and is sometimes referred to as a Type IV ELM in the community).

II. Description of high performance regime

The NSTX is a medium-sized, low aspect ratio spherical tokamak[13] with the following parameters: major radius R=0.85m, minor radius a=0.67m, R/a ≥ 1.26, toroidal field $B_t \leq 0.6$ T, with up to 7MW of NBI power (P_{NBI}) and 6 MW of radio-frequency heating. The basic characteristics of the NSTX high performance, small ELM regime are shown in Fig. 1 for a lower-single null diverted discharge with I_p=0.8 MA, B_t=0.5 T, P_{NBI} = 4.1 MW, elongation $\kappa \sim 1.9$, lower triangularity $\delta_L \sim 0.5$, and upper triangularity $\delta_U \sim$ 0.3. The line-average density continuously rises after the H-mode transition at t=230ms (Fig. 1b). Type V ELMs with a frequency ~ 400 Hz can be observed on the lower divertor D_α starting at t ~ 340 ms, although a few irregularly spaced type V ELMs are observed near 290 and 320 ms. Gas puffing from the center stack lasts throughout the discharge (Fig. 1c); the combination of this fueling and the NBI particle source contribute to the observed density rise. The stored energy remains flat for about 370 ms or ~ 7 energy confinement times (τ_E), and the confinement enhancement over ITER-89P scaling[14] is steady at ~ 2.3. For reference the steady β_p was ~ 1.2 (bootstrap current fraction 40-50%) and the line-average density relative to Greenwald scaling[15] ($n_{GW} = I_p/\pi a^2$) was 0.85 just before the end of the discharge, which was terminated by I_p ramp-down.

We note that details of this high performance regime for similar discharges have been reported previously[16-19]. The new interpretation presented in this paper pertains to 1) the positive identification of the D_α oscillations as tiny ELMs, which are different from ELMs in the published literature, and 2) the recent observation of conventional Type II/III ELMs in NSTX which confirm the uniqueness of these type V ELMs.

III. ELM characteristics

Many ELM types, including Type I, II/III, and the new Type V, have been observed[20] in NSTX. Fig. 2 contrasts the characteristics of these ELM types. The stored energy fractional drop (computed from reconstructions with the EFITD code[21] applied to NSTX[22] with a 0.25 ms time resolution) is typically between 5-15% for Type I ELMs (Fig. 1, row (a)), between 1-4% for Type II/III ELMs (Fig. 1, row (b)), and less than 1% for Type V ELMs (Fig. 1, row (c)) . There is some ambiguity in identifying the ELM type in row (b): these ELMS were observed only near the L-H power threshold (i.e. similar to Type III)[11] and only at an elongation > 2 in a shape very close to, but not quite a balanced double-null (i.e. similar to Type II)[23, 24]. Each of these ELM Types can also be observed in the far edge USXR data in the right hand column of Fig. 2, with Type I ELMs having the largest impact. The Type V ELMs increased the entire divertor D_α profile (Fig. 3) by ~ 20-30%, similar to the impact observed in the spatially integrated channel in panel 1(b). Note that that these ELMs were not the result of a long-lived coherent MHD mode. Low-n intermediate frequency (20-40 kHz) coherent modes (Fig. 4) were observed in the core from 300-700 msec, but these modes began after the type V ELM activity. In other discharges it was observed that these coherent modes persisted even after the ELMs stopped. Thus it is unlikely that the core modes are the source of the ELMs.

Insight into the ELM size, affected spatial depth and spatial origin can be obtained through examination of the USXR profile data[25]. At the time of these experiments, three arrays were implemented on NSTX: one each looking into the lower and upper divertors, and one looking from the top across the entire poloidal cross section (Fig. 5). The chords are spaced approximately 3 cm apart, and 5 μm Be foil filters were used to focus on emission from the edge of the plasma for the lower divertor and vertical arrays, whereas the upper divertor array had a 100 μm Be foil filter to focus on core USXR emission. The data were sampled at 190 kHz. For the vertical array, the chord numbering starts at 0 for

the chord nearest the outer midplane and increases to 17 for the chord nearest the inner midplane. For the lower divertor array, the chord numbering starts at 0 for the lowest chord and increases to 15 for the chord near the midplane. A thick filter was used on the upper divertor array to verify that the ELMs did not extend into the core.

Fig. 6a shows the relative change in intensity before and during a typical type V ELM. For reference, the statistical variability in the USXR signal is between 1-2% for this time, so relative changes in intensity of > 2% are significant. It can be seen that the chords 1-4 show the most significant change due to the ELM. Note that all USXR data presented here are line-integrated measurements, so changes in the edge chord emission are also seen to a lesser extent on adjoining chords. Hence the affected region is either one or two chords, i.e. a very narrow region of the plasma on the outboard side. Fig. 6b shows a (contrast enhanced) contour plot of several Type V ELMs from the vertical array. Note that the oscillation (e.g. the event near t=0.444 s) first appears on ~ chord 5, and propagates to chord 0 and then disappears for several 10s of □s. Fig. 6c shows the same events on the lower divertor array. In the time the perturbation disappears from the view of the vertical array, it appears in ~ chord 4 of the lower divertor array and then propagates rapidly to chord 15. Shortly after disappearing from the lower divertor array, the ELM reappears in chord 0 of the vertical array and propagates to chord 5 before dissipating. The geometry of the vertical array misses the plasma at the outer midplane, hence the disappearance of the ELM on that array signifies propagation to the outer midplane at the time. Simple triangulation indicates that the ELM is first observed in the lower divertor region at the USXR toroidal location, possibly in the vicinity of the X-point, and then propagates with a poloidal component to the outer midplane and then back around to the top of the machine. The duration of this perturbation on the USXR is ~ 200-500 □s, and the USXR perturbation precedes the divertor $D_{\square}$ light enhancement by a few 100 □s, indicating that the diagnostics indeed observe the same perturbation, the USXR on closed field lines and then the $D_{\square}$ after the perturbation crosses the separatrix to open field lines.

Near the onset of the perturbation in the USXR, a rotating mode with toroidal mode number n=1 is observed in the toroidal and poloidal Mirnov arrays (Fig. 7) below the outer midplane. This mode persists for about two toroidal transit times before the Type V ELM crash and propagates in the counter I_p direction. In comparison, higher-n

modes are sometimes observed for 200-300 μs prior to Type I ELM crashes, and coherent mode activity is observed for up several ms before a Type II/III ELM crash. We note that preliminary edge stability calculations were inconclusive for the Type V ELMs, with computed limits depending strongly on the assumed H-mode edge current density and pressure profile gradients. Near term improvements to the spatial resolution of edge diagnostics as well as the measurement of the magnetic field pitch via the motional Stark effect will allow a more thorough assessment of the edge stability in these discharge scenarios.

IV. Particle control aspects

One critical question is the ability of the Type V ELMs to provide sufficient density and impurity control. Experimentally it is observed that the edge carbon density and radiation increased during these discharges, but the core radiated power and Z_{eff} remained low. Part of the density rise may have been the result of continuous fueling from the center stack gas injection system, which has a ~ 500ms e-folding on the fueling rate after activation. The density rise from #108729 was examined via a simple particle balance model.:

$$\frac{dN}{dt} = \eta_{NBI} S_{NBI} + \eta_{gas} S_{gas}(t) - \frac{N}{\tau_p^*} \qquad (1)$$

Here N is the particle content inside the separatrix, S_{NBI} and $S_{gas}(t)$ are the NBI and gas fueling rates, η_{NBI} and η_{gas} are the NBI and external gas direct fueling efficiencies, and τ_p^* is the particle containment time. The gas fueling rate from the center stack is given by:

$$S_{gas}(t) = S_{gas,0} \exp\left(-\frac{t}{\tau_{gas}}\right) \cdot \tau_{gas} \sim 0.55\,\text{sec} \qquad (2)$$

The density rise ($\Delta N(t)$) following a step change in particle confinement at the L-H transition is obtained analytically by solving Eqn. (1):

$$\Delta N(t) = \left[\Gamma_{NBI} S_{NBI} \tau_p^* N_o \left(1 - \exp\left(-\frac{t}{\tau_p^*}\right)\right) + \frac{\Gamma_{gas} S_{gas,0} \tau_{gas} \tau_p^*}{\tau_{gas} - \tau_p^*} \exp\left(-\frac{t}{\tau_{gas}}\right) - \exp\left(-\frac{t}{\tau_p^*}\right)\right] \quad (3)$$

Assuming that the fueling efficiencies don't change appreciably during the density rise, the time dependence of the density can be fit to obtain τ_p^*~0.5 s, yielding a τ_p^*/τ_E~9. We caution that solution in Eqn. (3) has a mathematical singularity when τ_p^* approaches τ_{gas}, and that the fitting interval was approximately 1 X τ_p^*, limited by the pulse length. Nonetheless, we note that this value is approximately the same value obtained in DIII-D long pulse H-modes before active divertor pumping was enabled; the DIII-D ratio was reduced ~ 50% (by reducing τ_p^*) with efficient in-vessel cryo-pumping (i.e. line average density was reduced by at least a factor of 2)[26]. We also note that the density rises even more quickly in NSTX ELM-free discharges than in discharges with type V ELMs. Thus it is probable that NSTX could achieve a similar reduction in τ_p^*/τ_E with an efficient active pumping scheme, implying that the particle confinement reduction provided by these ELMs will allow for sufficient density control.

V. Summary, Discussion and Conclusions

We have observed a high performance regime in NSTX which is compatible with tiny ELMs with a frequency ~ 300 – 800 Hz. The stored energy drop per type V ELM is not statistically measurable, i.e. < 1%. The perturbations are visible in the USXR diagnostic, which precedes the D_α burst in the divertor. There is no clear P_{NBI} scaling, although these ELMs disappear and Type II/III ELMs are observed with P_{NBI} < 2.5 MW in certain discharge shapes. The Type V ELMs are observed with P_{NBI} up to 6.2 MW, and occasionally larger Type I ELMs co-exist with these ELMs. There is a clear electromagnetic n=1 pre-cursor rotating counter to the plasma current before the Type V ELM crash.

Type V ELMs have clear differences compared with published ELM types, many of which have also been observed in other NSTX discharges. Some of the highest power

NSTX discharges also have Type I ELMs mixed in with Type V ELMs, but Type II/III ELMs are observed with different discharge shapes. The NSTX type V ELMs are observed at medium to high density (between 0.5 and 1 X n_{GW}, with typical pedestal collisionality ≥ 1). The compatibility of Type V ELMs with high performance plasmas and the calculations showing that density control would be possible with active pumping make this operating regime an attractive possibility for next generation devices. Extrapolation of this regime to conventional aspect ratio tokamaks and a theoretical explanation of the instability mechanism are being explored.

Acknowledgements

This research was supported by the U. S. Dept. of Energy under contracts DE-AC05-00OR22725, DE-AC02-76CH03073 and W-7405-ENG-36, and grants DE-FG02-99ER54519, DE-FG02-99ER54523, and DE-FG02-99ER54524, We gratefully acknowledge the contributions of the NSTX operations staff.

Figure Captions

1. High performance discharge with Type V ELMs: (a) I_p and P_{NBI}, (b) line-averaged density (n_e) and lower divertor D_α emission, (c) NBI (S_{NBI}) and gas (S_{gas}) fueling rates, and density rise rate (dN_e/dt), (d) stored energy (W_{MHD}) and energy confinement normalized to the ITER-89P scaling. The Type V ELMs start at t~0.34s as indicated by the vertical line.
2. Characteristics of different ELM types in NSTX: (a) Type I, (b) Type II/III, and (c) Type V.
3. ELMs observed as small perturbations on divertor D_α radial profile
4. Spectrum of instabilities with n=1-6 for #108729: coherent MHD activity in the core plasma begins at about 0.3s and persists during the type V ELM phase
5. USXR view geometry for #108729 @ 0.35 s.
6. USXR view of divertor ELM: (a) change in intensity before/during ELM, (b) contour plot of vertical USXR showing ELM propagation, and (c) contour plot of lower divertor USXR showing ELM propagation.
7. Magnetic signature of Type V ELMs: (a) divertor D_α, (b) expanded scale D_α, (c) magnetic perturbation size at wall at $\phi=30^0$, (d) toroidal Mirnov array with dark blue bands showing mode toroidal propagation counter to I_p, and (e) passive plate Mirnov array with dark blue bands showing mode poloidal propagation upward. The approximate mode birth is highlighted by circles in (d) and (e).

Figure 1

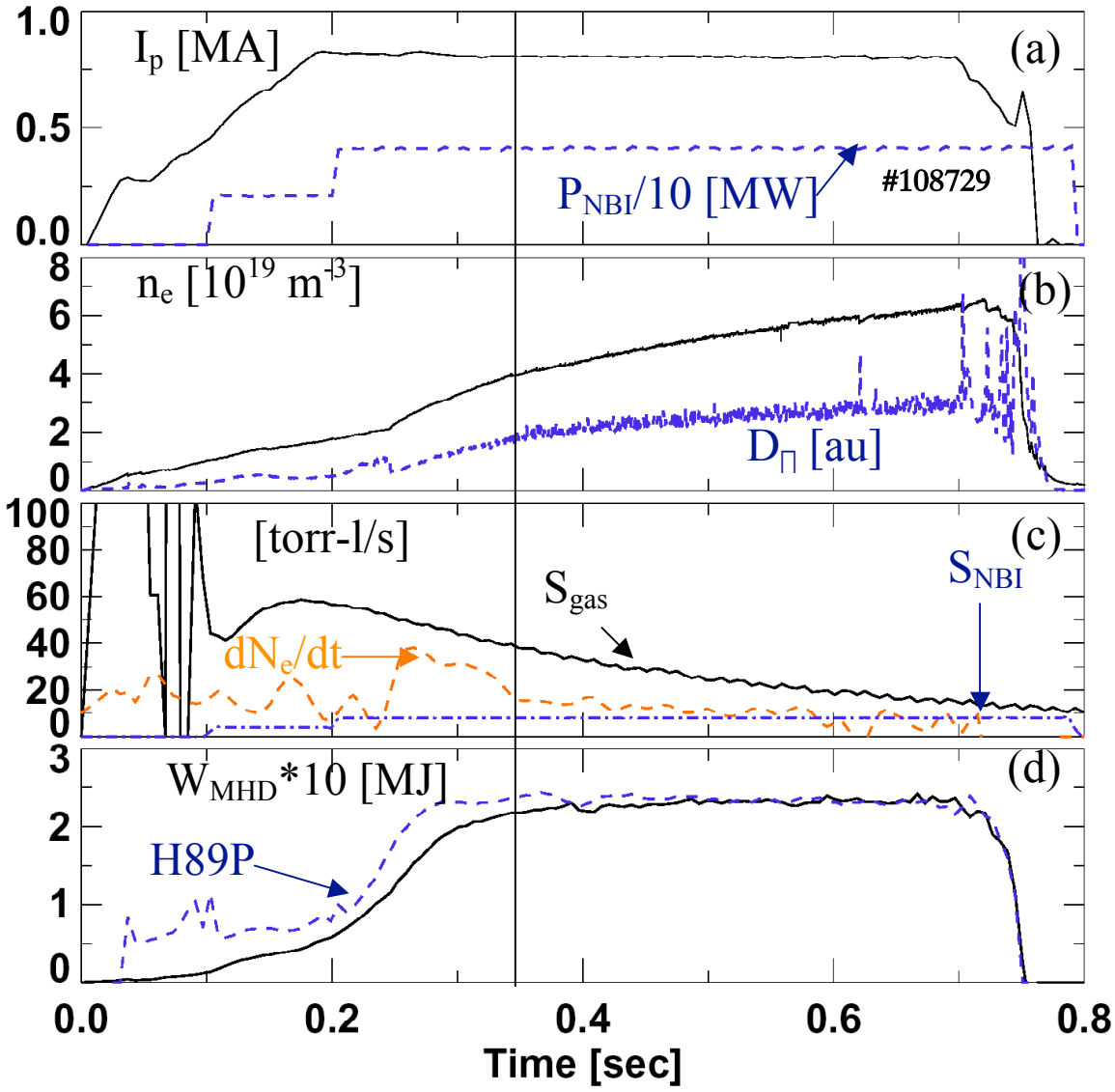
1.0
0.5
0.0
I_p [MA]
(a)
P_{NBI}/10 [MW]
#108729
8
6
4
2
0
n_e [10^{19} m^{-3}]
(b)
D_Π [au]
100
80
60
40
20
0
[torr-l/s]
(c)
S_{gas}
S_{NBI}
dN_e/dt
3
2
1
0
W_{MHD}*10 [MJ]
(d)
H89P
0.0
0.2
0.4
0.6
0.8
Time [sec]

Figure 2

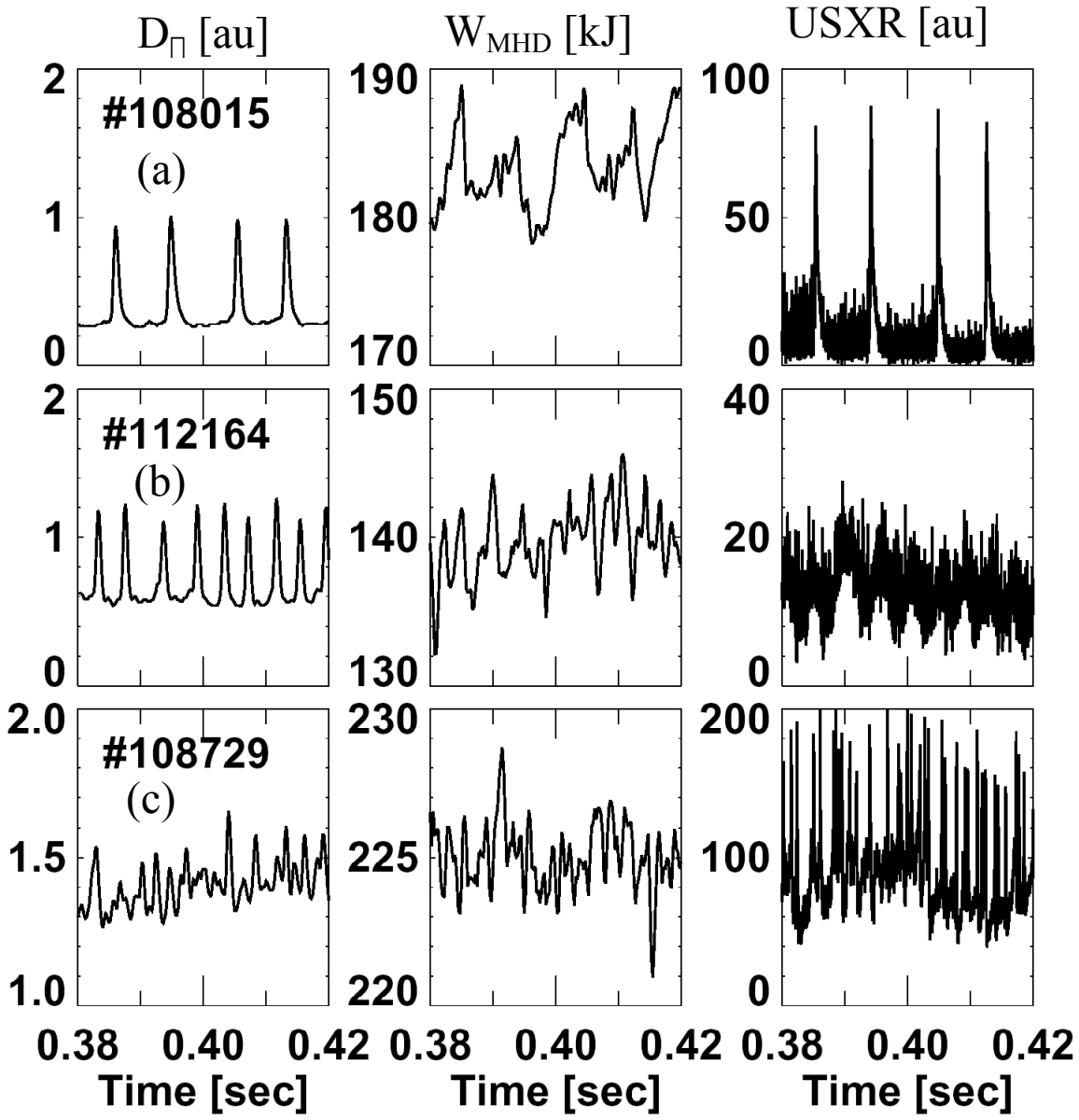
D∏ [au]
W MHD [kJ]
USXR [au]
#108015
(a)
#112164
(b)
#108729
(c)
2
1
0
190
180
170
100
50
0
150
140
130
40
20
2.0
1.5
1.0
230
225
220
200
100
0.38
0.40
0.42
Time [sec]

Fig. 3

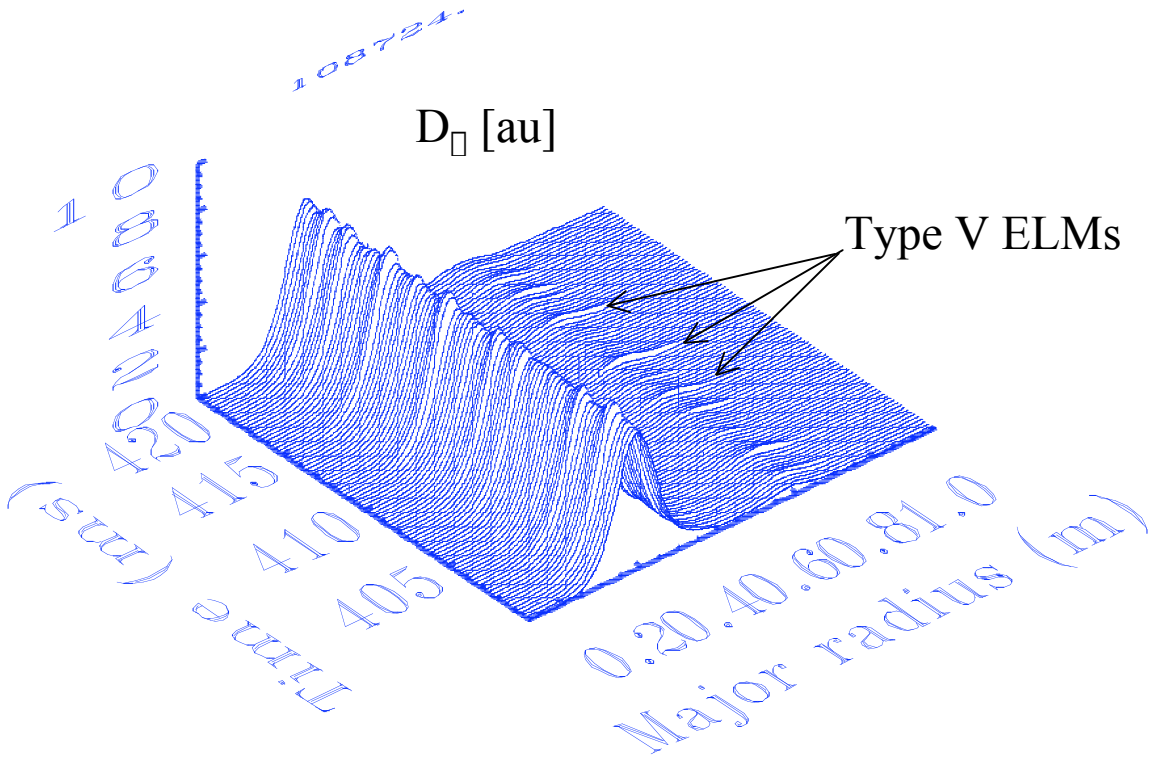

Figure 4

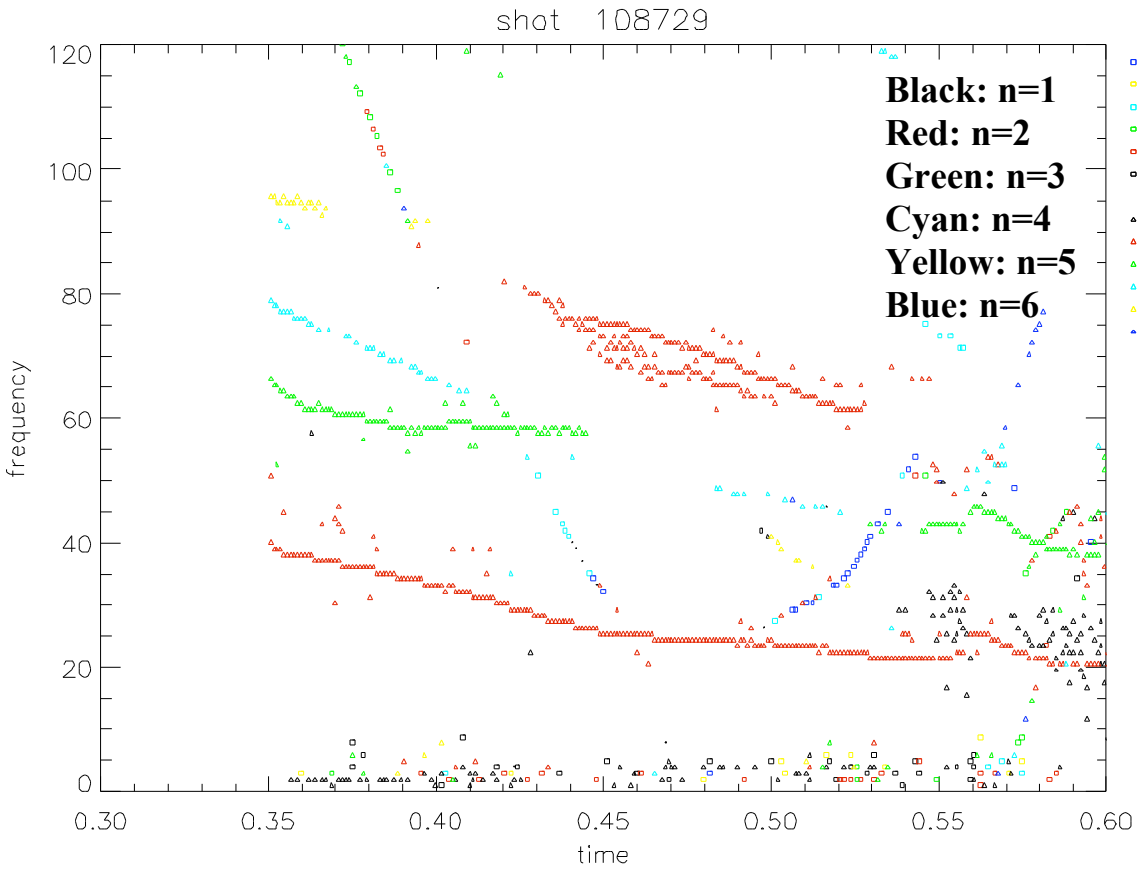
shot 108729
Black: n=1
Red: n=2
Green: n=3
Cyan: n=4
Yellow: n=5
Blue: n=6
frequency
time
0
20
40
60
80
100
120
0.30
0.35
0.40
0.45
0.50
0.55
0.60

Figure 5

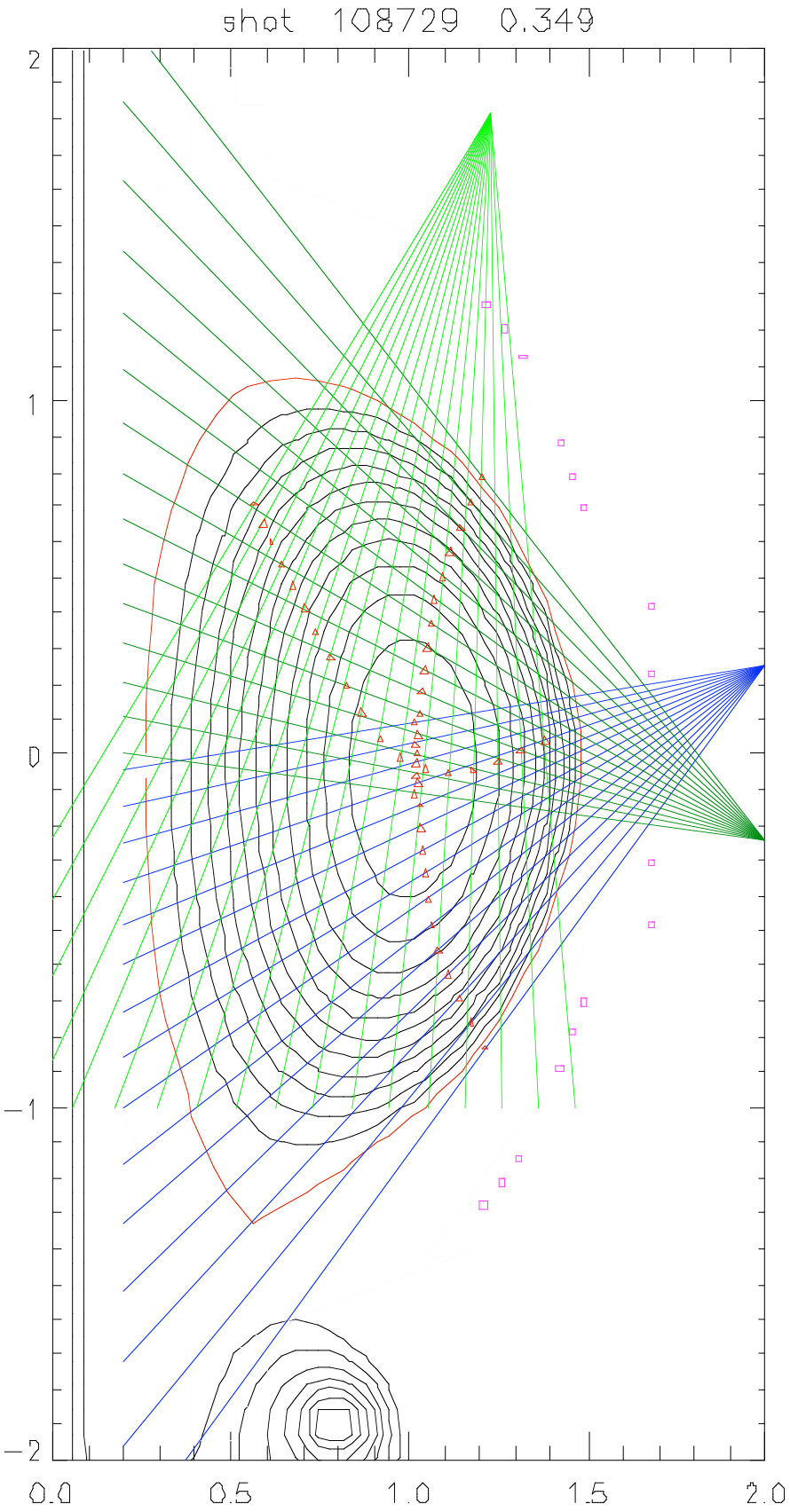

Figure 6a – SXR picture of outboard Type V ELM (from #108730)

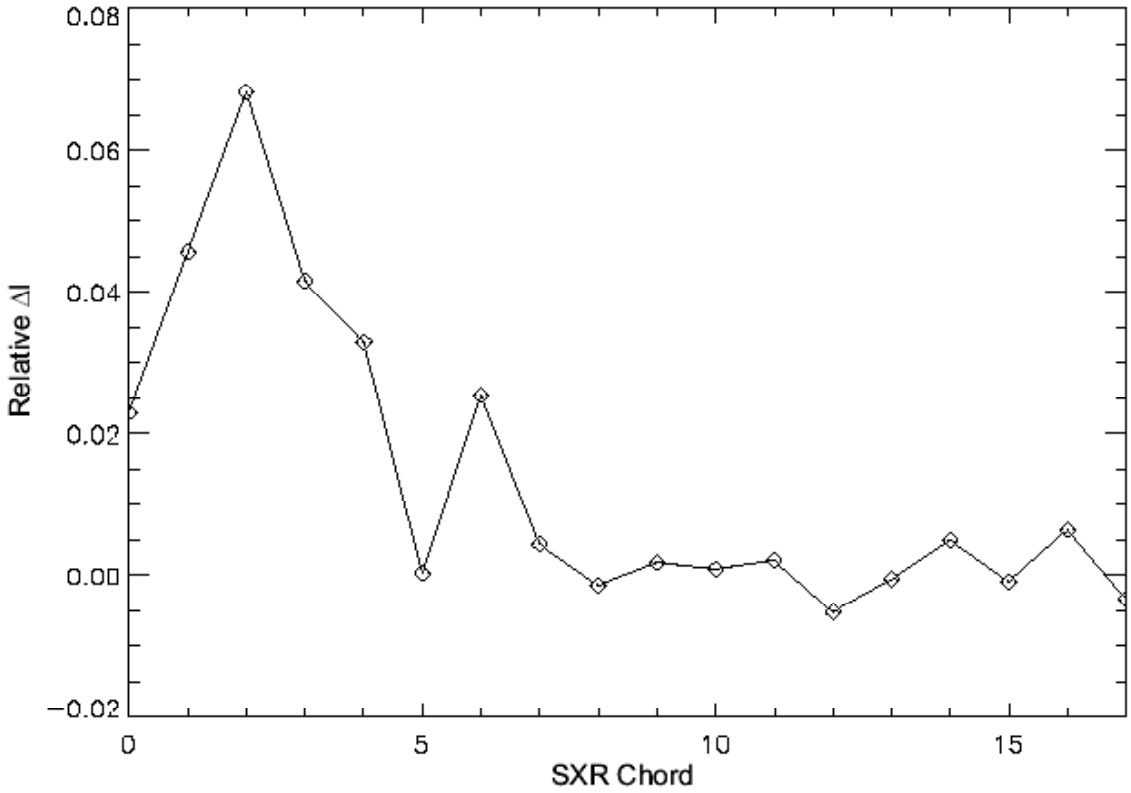

Outboard Center Inboard

Figure 6b,c (USXR top, lower divertor contours)

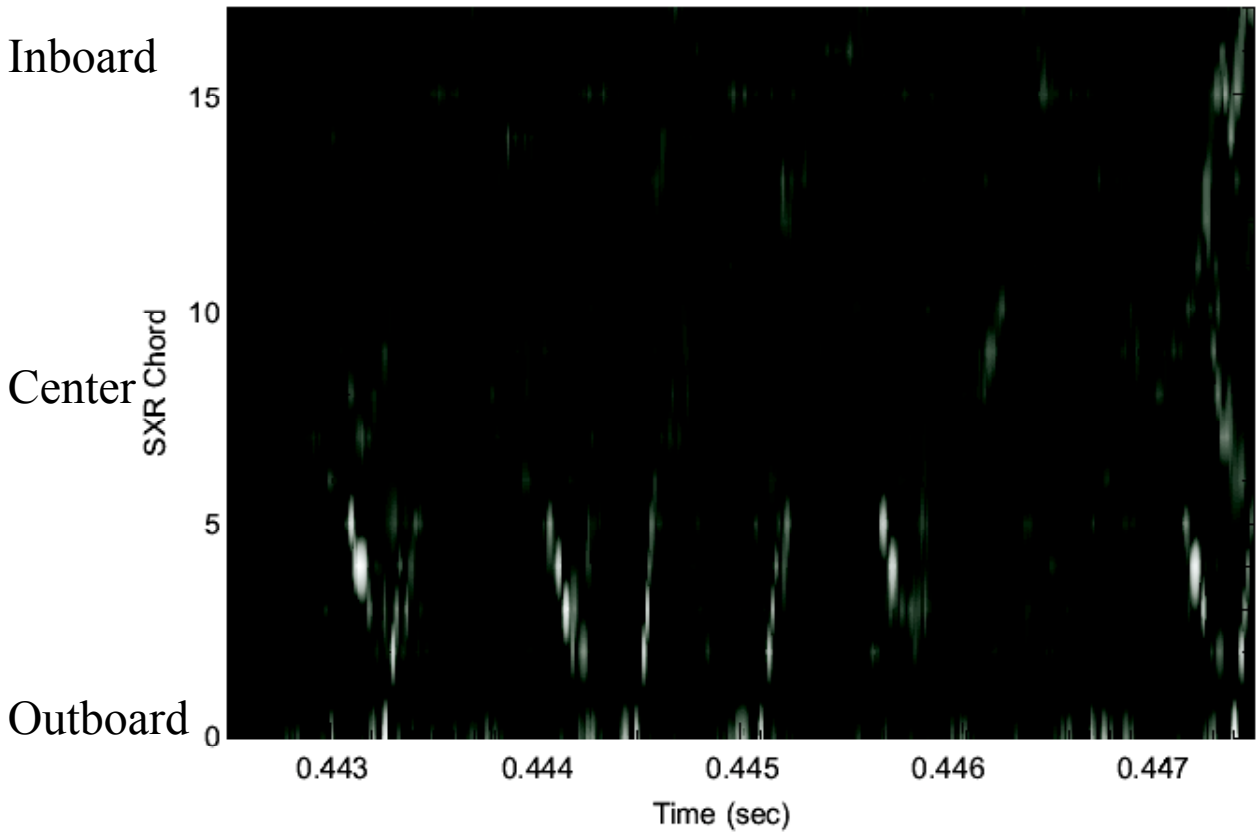

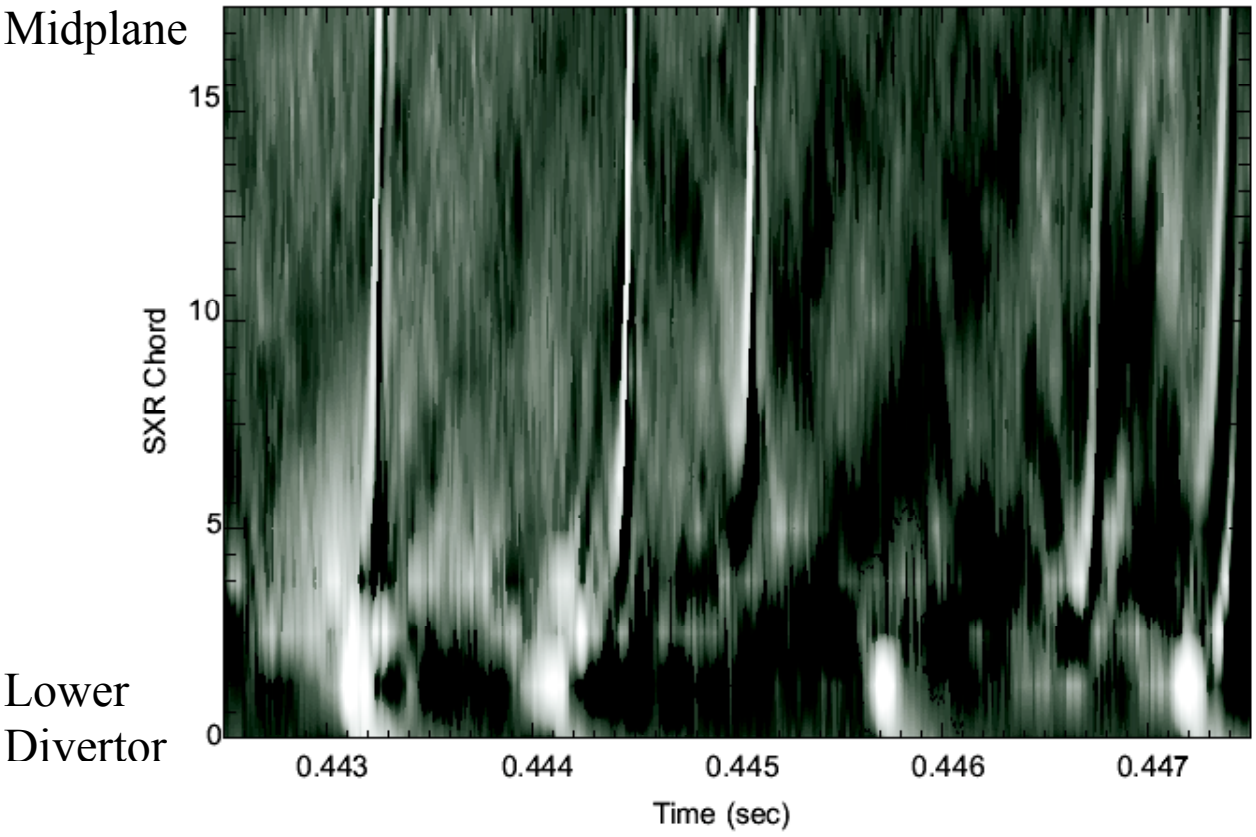

Figure 7

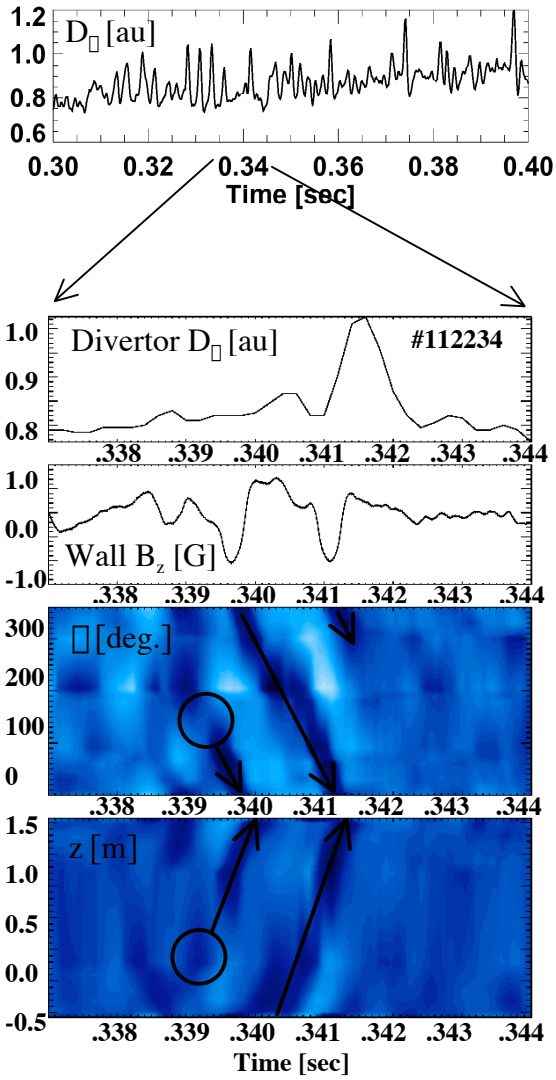
1.2
1.0
0.8
0.6
D□ [au]
0.30
0.32
0.34
0.36
0.38
0.40
Time [sec]
1.0
0.9
0.8
Divertor D□ [au]
#112234
.338
.339
.340
.341
.342
.343
.344
1.0
0.0
-1.0
Wall Bz [G]
300
200
100
0
□ [deg.]
1.5
1.0
0.5
0.0
-0.5
z [m]
Time [sec]

References

[1] I. P. B. Authors, et. al., Nuclear Fusion 39, (1999)2137.
[2] A. Loarte, et. al., J. Nucl. Materials 313-316, (2003)962.
[3] G. Federici, et. al., J. Nucl. Materials 313-316, (2003)11.
[4] C. M. Greenfield, et. al., Physical Review Letters 86, (2001)4544.
[5] Y. Takase, et. al., Physics of Plasmas 4, (1997)1647.
[6] S. M. Kaye, et. al., J. Nucl. Materials 121, (1984)115.
[7] K. Kamiya, et. al., Nuclear Fusion 43, (2003)1214.
[8] Y. Kamada, et. al., Plasma Physics Controlled Fusion 42, (2000)A247.
[9] Y. Kamada, et. al., Plasma Physics Controlled Fusion 44, (2002)A279.
[10] T. E. Evans, et. al., Physical Review Letters 92, (2004)article #235003.
[11] E. J. Doyle, et. al., Physics of Fluids B 3, (1991)2300.
[12] T. H. Osborne, et. al., Proc. of the 24th European Conference on Controlled Fusion and Plasma Physics, Berchtesgaden, Germany 1997 (EPS, Petit-Lancy, Switzerland), (1997).
[13] M. Ono, et. al., Nuclear Fusion 40, (2000)557.
[14] P. N. Yushmanov, et. al., Nuclear Fusion 30, (1990)1999.
[15] M. Greenwald, et. al., Nuclear Fusion 28, (1988)2199.
[16] D. A. Gates, et. al., Physics of Plasmas 10, (2003)1659.
[17] J. E. Menard, et. al., Nuclear Fusion 43, (2003)330.
[18] R. Maingi, et. al., Plasma Physics Controlled Fusion 45, (2003)657.
[19] S. A. Sabbagh, et. al., Physics of Plasmas 9, (2002)2085.
[20] R. Maingi, et. al., J. Nucl. Materials, (at press).
[21] L. L. Lao, et. al., Nuclear Fusion 25, (1985)1611.
[22] S. A. Sabbagh, et. al., Nuclear Fusion 41, (2001)1601.
[23] T. Ozeki, et. al., Nuclear Fusion 30, (1990)1425.
[24] J. Stober, et. al., Nuclear Fusion 41, (2001)1123.
[25] D. Stutman, et. al., Review of Scientific Instruments 74, (2003)1982.
[26] M. A. Mahdavi, et. al., J. Nucl. Materials 220-222, (1995)13.

External Distribution

Plasma Research Laboratory, Australian National University, Australia

Professor I.R. Jones, Flinders University, Australia

Professor João Canalle, Instituto de Fisica DEQ/IF - UERJ, Brazil

Mr. Gerson O. Ludwig, Instituto Nacional de Pesquisas, Brazil

Dr. P.H. Sakanaka, Instituto Fisica, Brazil

The Librarian, Culham Laboratory, England

Mrs. S.A. Hutchinson, JET Library, England

Professor M.N. Bussac, Ecole Polytechnique, France

Librarian, Max-Planck-Institut für Plasmaphysik, Germany

Jolan Moldvai, Reports Library, Hungarian Academy of Sciences, Central Research Institute for Physics, Hungary

Dr. P. Kaw, Institute for Plasma Research, India

Ms. P.J. Pathak, Librarian, Institute for Plasma Research, India

Ms. Clelia De Palo, Associazione EURATOM-ENEA, Italy

Dr. G. Grosso, Instituto di Fisica del Plasma, Italy

Librarian, Naka Fusion Research Establishment, JAERI, Japan

Library, Laboratory for Complex Energy Processes, Institute for Advanced Study, Kyoto University, Japan

Research Information Center, National Institute for Fusion Science, Japan

Dr. O. Mitarai, Kyushu Tokai University, Japan

Dr. Jiangang Li, Institute of Plasma Physics, Chinese Academy of Sciences, People's Republic of China

Professor Yuping Huo, School of Physical Science and Technology, People's Republic of China

Library, Academia Sinica, Institute of Plasma Physics, People's Republic of China

Librarian, Institute of Physics, Chinese Academy of Sciences, People's Republic of China

Dr. S. Mirnov, TRINITI, Troitsk, Russian Federation, Russia

Dr. V.S. Strelkov, Kurchatov Institute, Russian Federation, Russia

Professor Peter Lukac, Katedra Fyziky Plazmy MFF UK, Mlynska dolina F-2, Komenskeho Univerzita, SK-842 15 Bratislava, Slovakia

Dr. G.S. Lee, Korea Basic Science Institute, South Korea

Institute for Plasma Research, University of Maryland, USA

Librarian, Fusion Energy Division, Oak Ridge National Laboratory, USA

Librarian, Institute of Fusion Studies, University of Texas, USA

Librarian, Magnetic Fusion Program, Lawrence Livermore National Laboratory, USA

Library, General Atomics, USA

Plasma Physics Group, Fusion Energy Research Program, University of California at San Diego, USA

Plasma Physics Library, Columbia University, USA

Alkesh Punjabi, Center for Fusion Research and Training, Hampton University, USA

Dr. W.M. Stacey, Fusion Research Center, Georgia Institute of Technology, USA

Dr. John Willis, U.S. Department of Energy, Office of Fusion Energy Sciences, USA

Mr. Paul H. Wright, Indianapolis, Indiana, USA

The Princeton Plasma Physics Laboratory is operated
by Princeton University under contract
with the U.S. Department of Energy.

Information Services
Princeton Plasma Physics Laboratory
P.O. Box 451
Princeton, NJ 08543

Phone: 609-243-2750
Fax: 609-243-2751
e-mail: pppl_info@pppl.gov
Internet Address: http://www.pppl.gov